AMERICAN SOCIETY FOR MICROBIOLOGY | Journal of Virology®

CELLULAR RESPONSE TO INFECTION

African Swine Fever Virus Regulates Host Energy and Amino Acid Metabolism To Promote Viral Replication

Qiao Xue,[a] Huisheng Liu,[a] Zixiang Zhu,[a] Fan Yang,[a] Yingying Song,[b] Zongqiang Li,[c] Zhaoning Xue,[a] Weijun Cao,[a] Xiangtao Liu,[a] Haixue Zheng[a]

[a]State Key Laboratory of Veterinary Etiological Biology, National Foot and Mouth Diseases Reference Laboratory, Key Laboratory of Animal Virology of Ministry of Agriculture, Lanzhou Veterinary Research Institute, Chinese Academy of Agricultural Sciences, Lanzhou, China
[b]Shanghai Veterinary Research Institute, Chinese Academy of Agricultural Sciences, Shanghai, China
[c]State Key Laboratory of Membrane Biology, Beijing Advanced Innovation Center for Structural Biology, School of Life Sciences, Tsinghua University, Beijing, China

Qiao Xue, Huisheng Liu, and Zixiang Zhu contributed equally to this work. Author order was determined by funding sources.

ABSTRACT African swine fever is one of the most serious viral diseases caused by African swine fever virus (ASFV). The metabolic changes induced by ASFV infection remain unknown. Here, porcine alveolar macrophages (PAMs) infected with ASFV was analyzed by ultrahigh-performance liquid chromatography–quadrupole time-of-flight tandem mass spectrometry (UHPLC-QTOF-MS) in combination with multivariate statistical analysis. A total of 90 metabolites were significantly changed after ASFV infection, and most of them were amino acids and tricarboxylic acid (TCA) cycle intermediates. ASFV infection induced an increase in most of amino acids in the host during the early stages of infection, and amino acids decreased in the late stages of infection. ASFV infection did not significantly affect the glycolysis pathway, whereas it induced increases in citrate, succinate, α-ketoglutarate, and oxaloacetate levels in the TCA cycle, suggesting that ASFV infection promoted the TCA cycle. The activities of aspartate aminotransferase and glutamate production were significantly elevated in ASFV-infected cells and pigs, resulting in reversible transition between TCA cycle and amino acid synthesis. Aspartate, glutamate, and TCA cycle were essential for ASFV replication. In addition, ASFV infection induced an increase in lactate level using lactate dehydrogenase, which led to low expression of beta interferon (IFN-β) and increased ASFV replication. Our data, for the first time, indicate that ASFV infection controls IFN-β production through RIG-I-mediated signaling pathways. These data identified a novel mechanism evolved by ASFV to inhibit host innate immune responses and provide insights for development of new preventive or therapeutic strategies targeting the altered metabolic pathways.

IMPORTANCE In order to promote viral replication, viruses often cause severe immunosuppression and seize organelles to synthesize a large number of metabolites required for self-replication. African swine fever virus (ASFV) has developed many strategies to evade host innate immune responses. However, the impact of ASFV infection on host cellular metabolism remains unknown. Here, for the first time, we analyzed the metabolomic profiles of ASFV-infected PAMs. ASFV infection increased host TCA cycle and amino acid metabolism. Aspartate, glutamate, and TCA cycle promoted ASFV replication. ASFV infection also induced the increase of lactate production to inhibit innate immune responses for self-replication. This study identified novel immune evasion mechanisms utilized by ASFV and provided insights into ASFV-host interactions, which is critical for guiding the design of new prevention strategies against ASFV targeting the altered metabolic pathways.

KEYWORDS ASFV, metabolomics, TCA cycle, lactate, RIG-I

Editor Jae U. Jung, Lerner Research Institute, Cleveland Clinic

Address correspondence to Haixue Zheng, haixuezheng@163.com.

The authors declare no conflict of interest.

Received 5 November 2021
Accepted 1 December 2021
Accepted manuscript posted online 15 December 2021
Published 23 February 2022

African swine fever virus (ASFV), a member of the family *Asfarviridae* and genus *Asfivirus*, has a double-stranded DNA molecule of 170 to 190 kb expressing more than 150 proteins, which play important roles in viral replication, virus-host interactions, and immune evasion (1, 2). ASFV was originally isolated and identified in Kenya in the 1920s and has remained endemic in Africa (3). Subsequently, ASFV rapidly spread to Europe, including France, Spain, Italy, Portugal, Georgia, Ukraine, Moldova, Czech Republic, Romania, and Poland (4). Recently, ASFV has been identified and reported in more than 37 countries (5–7). Between the 1950s and 1980s, ASFV genotype I emerged in Europe, Russia, and South America. In 2007, ASFV genotype II emerged in Georgia and continued to spread to more countries (8).

In China, the first case of ASFV infection was reported in Liaoning Province in 2018 and was characterized by obvious enlargement of the spleen and generalized hemorrhage in pigs (5, 9, 10). ASFV infections were subsequently reported in many provinces in China. ASFV has threatened more than 50% of the domestic pig population in China, causing severe economic losses (5). So far, most ASFV isolates in China belong to genotype II (10).

The innate immune response is the first line of the host's defense against viral infection. Viruses also negatively regulate the host innate immune response to promote self-replication. To facilitate virus replication in host cells, viruses can seize organelles to synthesize a large number of metabolites required for viral replication (11, 12). For instance, Newcastle disease virus (NDV) (12), influenza A virus (IAV) (13), and human cytomegalovirus (HCMV) (14) have been proven to alter host cell metabolism for viral replication. Understanding the impact of viral infection on host cell metabolism will promote knowledge of pathogenic mechanisms and contribute to advancing novel preventative measures targeting metabolism. Metabolomics is a new approach to identifying the special small metabolites of diseases in cancer and other diseases and has already been widely used in biological studies of animals, humans, and plants (15–19). ASFV infection can control the cGAS-STING pathway and regulates beta interferon (IFN-β) production (20, 21). Studies have indicated that some ASFV proteins inhibited host innate immune response to promote viral replication by different mechanisms (22–25). However, the intrinsic mechanisms of the interaction between ASFV and host cell metabolism remain unknown.

In the present study, ASFV-infected PAMs were collected and subjected to metabolomic analysis using ultrahigh-performance liquid chromatography/quadrupole time-of-flight tandem mass spectrometry (UHPLC-QTOF-MS). Mock-infected cells were used as controls. The results showed that ASFV infection altered host energy and amino acid metabolism, both *in vitro* and *in vivo*. The tricarboxylic acid (TCA) cycle, aspartate, and glutamate play important roles in ASFV replication. ASFV infection enhanced lactate production to inhibit host IFN-β expression and promote viral replication. The RIG-I-mediated signaling pathway was involved in ASFV-induced IFN-β production.

RESULTS

Multivariate analysis of PAM metabolites. To analyze metabolites in porcine alveolar macrophages (PAMs) infected by ASFV, we first confirmed ASFV replication in PAMs. Viral titer was significantly upregulated as the infection progressed, and no significant differences were observed between 24 and 48 h postinfection (hpi) (Fig. 1A), which indicated that growth almost reached saturation after 24 hpi, showing a high percentage of infection. The expression of P30 protein was determined by Western blotting. P30 protein also increased over time (Fig. 1B). These results indicated the successful replication of ASFV in PAMs. To further evaluate the cell states during ASFV infection, apoptosis was detected by the terminal deoxynucleotidyl transferase-mediated dUTP nick end labeling (TUNEL) assay. Apoptosis increased significantly as the infection progressed, and more than 95% of cells were observed to undergo apoptosis at 48 hpi (Fig. 1C).

Electrospray ionization is the source of UHPLC-QTOF-MS and contains positive

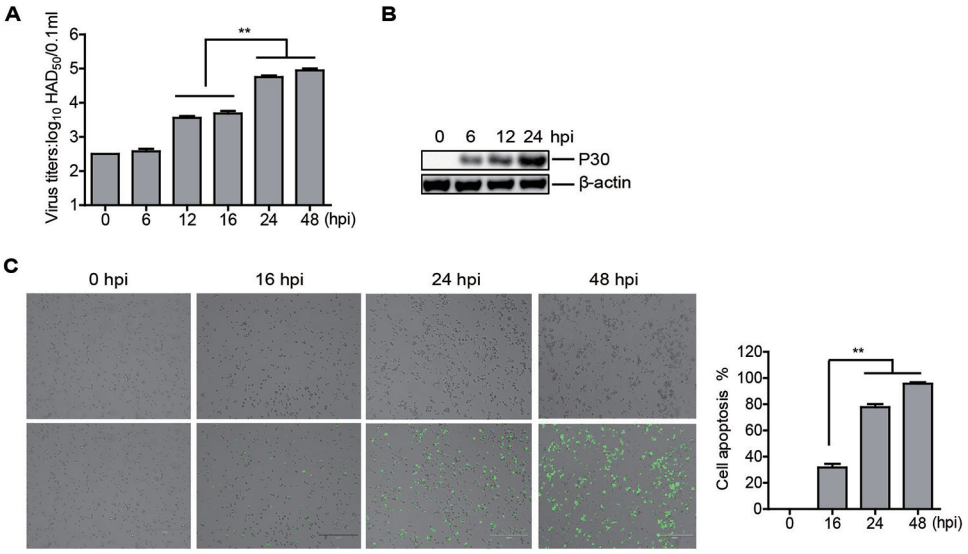

FIG 1 Detection of ASFV replication in PAMs. PAMs were infected with ASFV (MOI, 1) for 0, 6, 12, 16, 24, or 48 h. The cells and cell culture supernatants were frozen and thawed three times to release the virus and then were centrifuged at 1,200 rpm for 5 min. The supernatants were collected, and the viral titers were determined by HAD_{50} assay (A). Expression of viral P30 protein was detected by Western blotting (B). (C) PAMs cultured in 12-well plates were infected with ASFV (MOI, 1) for 0, 16, 24, or 48 h. Cellular apoptosis was detected by TUNEL assay using a one-step TUNEL apoptosis detection kit. The apoptosis rate of cells was analyzed with ImageJ software.

(POS) and negative (NEG) ion modes. The valid peaks were matched for 302 (POS) and 185 (NEG) PAM metabolites, according to an in-house MS2 database and the KEGG Compound Metabolomics Library. We then analyzed nonorthogonal and orthogonal variables using orthogonal partial least-squares discrimination analysis (OPLS-DA). The OPLS-DA data for the mock-infected and infected groups are shown in Fig. 2. Taken together, these results indicated that the infection model was reliable and stable.

Significant changes in metabolites were observed following ASFV infection in PAMs. The differential metabolites are shown in the form of volcano plots (Fig. 3). Each point in the volcanic map represents a metabolite. Changes of $>$1.5-fold or $<$0.67-fold and *P* values from Student's *t* test ($P < 0.05$) are displayed.

A total of 90 metabolites were significantly changed after ASFV infection. Relative to values recorded at 0 h, 65 metabolites were significantly upregulated and 25 metabolites were significantly downregulated (Fig. 4A). A significant difference was observed in the heat map depicting hierarchical clustering of the metabolite data (Fig. 4B). The number of upregulated metabolites increased gradually over time. There was an increase in the levels of many amino acids which are associated with amino acid metabolism. Taken together, these results indicated that ASFV infection induced significant differential metabolites.

Analysis of metabolites and metabolic pathways. The KEGG Metabolome Database and MetaboAnalyst were used to search the corresponding pathway database of the pig and further identify the corresponding pathway database related to the changes in metabolites. The results of the metabolic pathways analysis are shown by a bubble plot (Fig. 5). There were many altered metabolic pathways during the progress of ASFV infection. Pathway impact values suggested that the main enrichment metabolic pathways of differential metabolites during ASFV infection included aminoacyl-tRNA biosynthesis, alanine, aspartate, and glutamate metabolism, arginine biosynthesis, biosynthesis of amino acids, and protein digestion and absorption.

The detailed profiles of the metabolite changes in PAMs infected with ASFV were obtained using UHPLC-QTOF-MS (Fig. 6). Amino acids, an important substrate, are essential to cell metabolism and proliferation. In the present study, at 6 hpi, a few metabolites, including histidine, UMP, and glutamine, were affected. At 24 hpi, the levels of histidine, serine, alanine, aspartate, glutamate, arginine, and lactate were significantly upregulated, which was consistent with the viral replication process. Meanwhile,

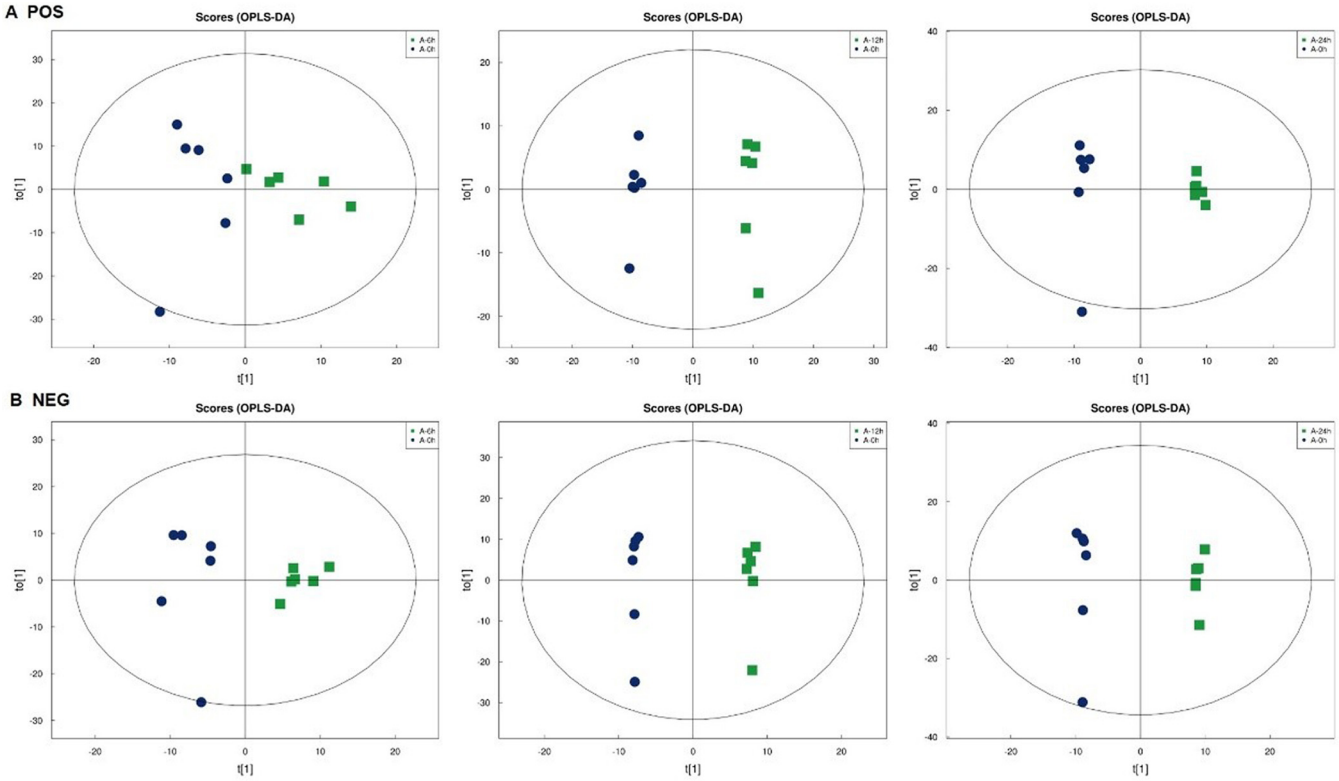

FIG 2 OPLS-DA model for the mock-infected and ASFV-infected cells at the indicated time points. The OPLS-DA model was obtained from the UHPLC-QTOF-MS metabolomic profiles of PAM samples (A and B). (A), POS; (B), NEG.

the level of phosphocholine was significantly downregulated. As a whole, ASFV infection remarkably affected amino acid metabolism, which allowed them to play important roles in many key metabolic pathways during ASFV infection.

Amino acid metabolism targeted by ASFV infection. To further analyze the changes in amino acid metabolism during ASFV infection, the amount of amino acids was quantified at different time points of infection. The ion peak areas of the metabolites were detected using UHPLC-MS. The measured value was compared with that for the standard substance. At 24 hpi, elevated amounts of amino acids, including aspartate, arginine, glycine, isoleucine, phenylalanine, proline, tyrosine, valine, lysine, glutamate, and glutamine, in the ASFV-infected cells were detected compared to those in the mock-infected cells. The levels of other amino acids were either unchanged or decreased (Fig. 7). Both UHPLC-QTOF-MS and UHPLC-MS results showed that the levels of aspartate, glutamate, and arginine were significantly enhanced after ASFV infection. These three upregulated amino acids may play important roles in ASFV replication.

At 48 hpi, except for cystine, all the amino acids were downregulated in ASFV-infected cells compared to mock-infected cells. Detailed statistics are shown in Table 1. These results indicated that in the early stages of infection, ASFV induced the increase of amino acids to promote viral replication; however, in the late stages of infection, cellular amino acids were depleted by ASFV, resulting in a decrease in amino acids.

The energy metabolism targeted by ASFV infection. Amino acid metabolism is always associated with energy metabolism. Therefore, we further analyzed the changes of glycolysis and TCA cycle during ASFV infection using UHPLC-MS. As shown in Table 2 and Fig. 8A, the level of fructose 6-phosphate was significantly downregulated, while the pyruvate level was significantly upregulated. As for the TCA cycle, we identified some important metabolites using UHPLC-MS, which indicated that ASFV infection induced the increase of citrate and succinate levels (Fig. 8B). The levels of α-ketoglutarate and oxaloacetate were further determined using specific kits. The results showed that the expression of α-ketoglutarate, α-ketoglutarate dehydrogenase,

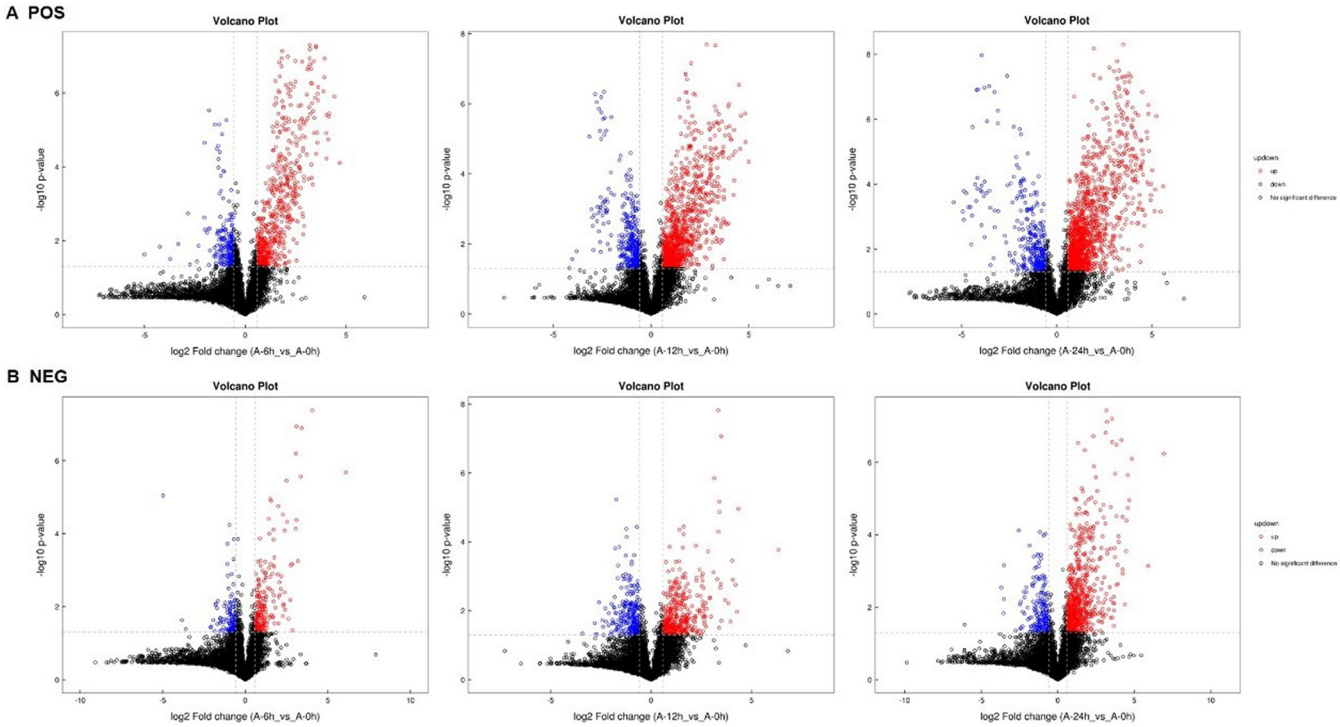

FIG 3 Volcano plots for the mock-infected and ASFV-infected cells at the indicated time points. Each point in the volcanic map represents a metabolite. Red, upregulation; blue, downregulation; gray, unchanged. (A), POS; (B), NEG.

and oxaloacetate was significantly upregulated as ASFV infection progressed (Fig. 8C). These results indicated that ASFV infection significantly affected the metabolites in the TCA cycle.

Aspartate aminotransferase (AST), a vitamin B_6-dependent enzyme, can promote the mutual transformation of aspartate and α-ketoglutarate to oxaloacetate and glutamate (26). To determine the relationship between aspartate and TCA cycle in the ASFV-infected cells and pigs, the activity of AST was identified during ASFV infection. In the ASFV-infected PAMs, the activity of AST was significantly enhanced as the infection progressed (Fig. 8D). The activity of AST was also significantly elevated in the serum of ASFV-infected pigs (Fig. 8E). Meanwhile, increased glutamate production was found both in ASFV-infected cells and the collected serum from ASFV-infected pigs (Fig. 8F). Taken together, these results indicated that ASFV infection promoted the TCA cycle, resulting in a reversible transition between TCA cycle and amino acid synthesis. The increased TCA cycle and amino acids may be associated with the replication and pathogenicity of ASFV.

Aspartate, glutamate, and TCA cycle promoted ASFV replication. As described above, ASFV infection induced an increase in partial amino acids and promoted the TCA cycle. Thus, we further detected the impact of aspartate, glutamate, and TCA cycle on ASFV replication. Tyrphostin 23 (T23) is a well-known inhibitor of protein tyrosine kinases, and the mitochondrial TCA cycle is strongly accelerated after T23 treatment (27). Thus, T23 was used to promote TCA cycle in the following experiment. The cytotoxicity of aspartate, glutamate, α-ketoglutarate, and the inhibitor was determined by the MTS assay. All doses of the inhibitor and metabolites used in the experiments showed no significant detectable cell death (data not shown).

PAMs cultured in six-well plate were infected with ASFV (multiplicity of infection [MOI], 1) and then incubated with increasing concentrations of aspartate, glutamate, α-ketoglutarate, or T23 for 24 h. Viral titers were determined by 50% hemadsorption (HAD_{50}) assay. Treatment with aspartate or T23 significantly promoted ASFV replication in a dose-dependent manner (Fig. 9). Treatment with 25 mg/L of glutamate or

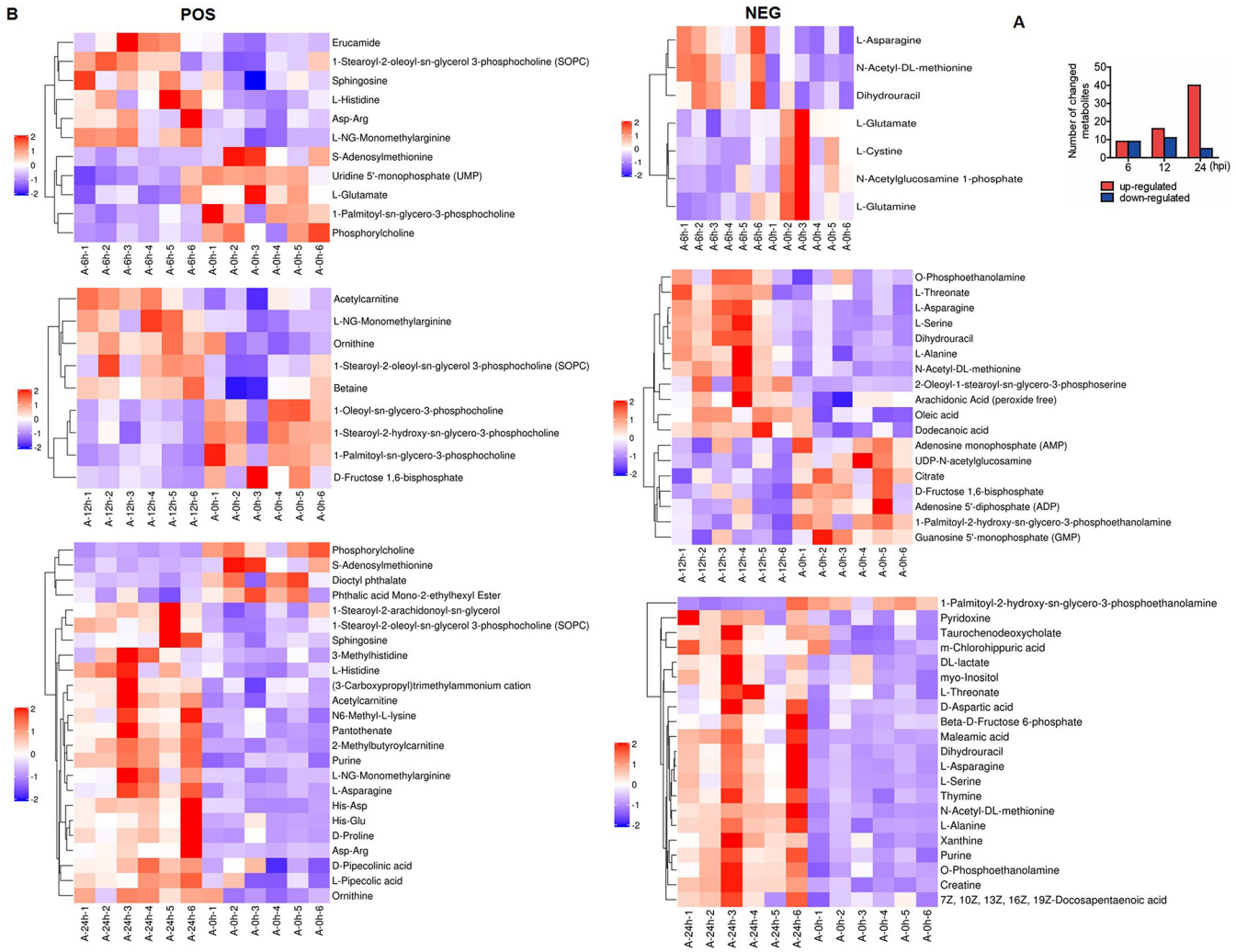

FIG 4 Significant changes in metabolites during ASFV infection. (A) Numbers of metabolites upregulated (red) and downregulated (blue) in ASFV-infected cells. (B) Heat map of hierarchical clustering analysis of differential metabolites. Each column represents one sample, and each row represents one differential metabolite. Red, upregulation; blue, downregulation.

α-ketoglutarate did not affect ASFV replication, while treatment with 50 mg/L of glutamate or α-ketoglutarate significantly promoted ASFV replication (Fig. 9). Together, these results indicated that cellular TCA cycle, aspartate, and glutamate play important roles in ASFV replication.

ASFV infection increased lactate production to promote viral replication. The UHPLC-QTOF-MS results showed that ASFV infection induced an considerable increase in lactate level. To confirm the impact of ASFV infection on lactate level, the expression of lactate during ASFV infection was determined using a lactate content detection kit. The level of lactate was significantly enhanced as the infection progressed (Fig. 10A). Lactate is a natural suppressor of RIG-like receptor (RLR) signaling by targeting mitochondrial antiviral-signaling (MAVS) protein (28). Thus, we detected the impact of lactate on ASFV-induced IFN-β expression. UK-5099 is an inhibitor of the mitochondrial pyruvate transporter and inhibits pyruvate-dependent O_2 consumption, promoting lactate production (29). Here, the level of lactate was significantly enhanced in the cells incubated with UK-5099 compared to that of mock-incubated cells (Fig. 10B), resulting in low expression of IFN-β induced by ASFV and increased replication of ASFV (Fig. 10C). GSK2837808A (GSK), a potent and specific inhibitor of lactate dehydrogenase (LDH), can inhibit lactate production (30). In contrast with UK-5099, GSK treatment induced low expression of lactate level (Fig. 10D), resulting in high expression of IFN-β

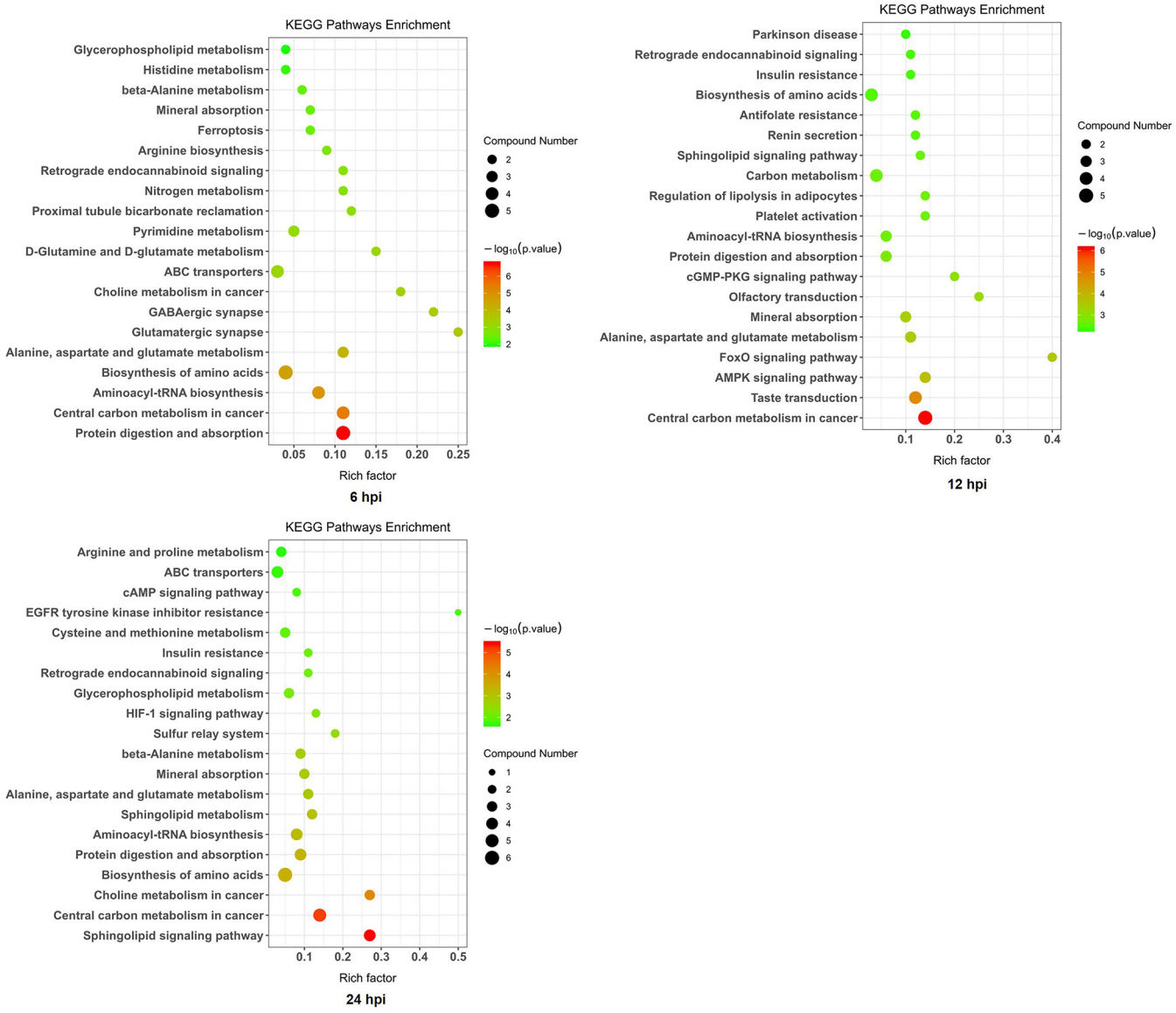

FIG 5 Bubble plots of the metabolic pathway analysis for ASFV-infected cells. Each bubble in the bubble diagram represents a metabolic pathway (the 20 with the highest significance, according to *P* value, are shown). The larger the bubble, the more metabolites there are. The *x* axis represents a pathway impact value in the topology analysis, and the size is positively correlated with the influence factor. The *y* axis represents the *P* value of the metabolic pathway in the enrichment analysis; the darker the color, the smaller the *P* value, indicating greater significance for the enrichment degree.

induced by ASFV and decreased replication of ASFV (Fig. 10E). All doses of UK-5099 and GSK used in the experiments also showed no significant detectable cell death (data not shown). LDH plays important roles in lactate production. Our results found that ASFV infection also improved the activity of LDH, which might directly contribute to the increase of lactate (Fig. 10F).

MAVS protein is a specific molecule in the RLR signaling pathway, while ASFV infection controls cGAS-STING pathway activation (20, 31). Thus, the impact of RIG-I on ASFV-induced IFN-β production was further investigated. PAMs cultured in 6-well plates were transfected with RIG-I and negative control (NC) small interfering RNA (siRNA) and infected with ASFV (MOI, 1). The secretion of IFN-β protein was significantly decreased in RIG-I siRNA cells compared to that in NC siRNA cells (Fig. 10G). Conversely, ASFV replication level was significantly enhanced in RIG-I siRNA cells compared to that in NC siRNA cells (Fig. 10G). The expression of RIG-I protein was confirmed by Western blotting. Altogether, these results indicated that ASFV infection induced an increase in lactate level, leading to the

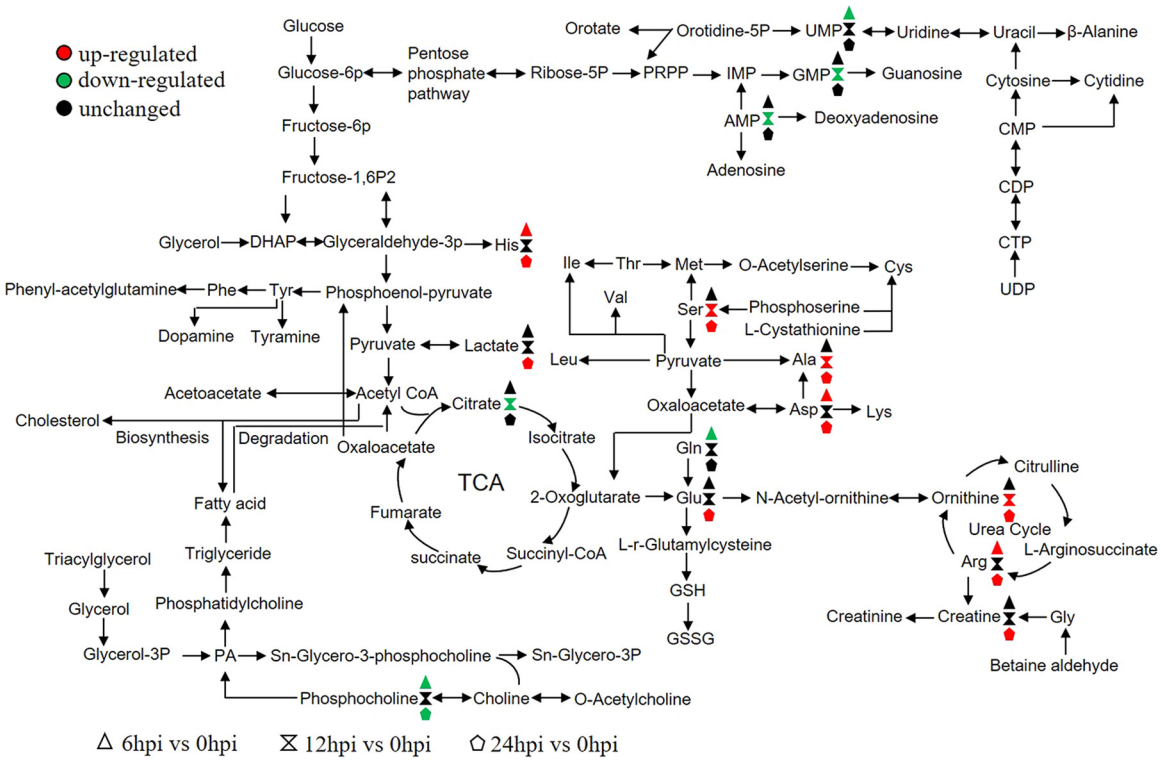

FIG 6 Schematic representation of altered metabolic pathways in PAMs infected with ASFV. Metabolomics of ASFV-infected PAMs was performed using UHPLC-QTOF-MS. Many metabolites and associated metabolic pathways were significantly altered after ASFV infection, including energy metabolism and amino acid metabolism. Red, upregulation; green, downregulation. Triangle, 6 hpi versus 0 hpi; hourglass, 12 hpi versus 0 hpi; pentagon, 24 hpi versus 0 hpi.

decreased expression of IFN-β and increased replication of ASFV, which revealed a novel mechanism evolved by ASFV to antagonize host innate immune responses. This is the first report showing that RIG-I is involved in ASFV-induced IFN-β activation.

DISCUSSION

In recent years, metabolomics has been made great achievements in understanding of metabolic change during viral infection. For instance, NDV infection mainly induces changes in cellular amino acid and nucleotide metabolism (12), IAV infection promotes self-replication by affecting metabolic pathways such as purine, lipid, and glutathione in host cells (13), and the central carbon metabolism, particularly glycolysis, is significantly altered in the context of dengue virus (DENV) infection, and depriving the exogenous glucose in DENV-infected cells has a pronounced impact on viral replication (32). Although many viruses regulate host metabolism to create beneficial environments for their own replication, different viruses regulate cell metabolism in different ways. It has become an important antiviral strategy to study the mechanism of the regulation of host cell metabolism by various viruses and design new preventive or therapeutic drugs targeting the altered metabolic pathways. In the present study, we for the first time analyzed the metabolomic profiles of ASFV-infected PAMs using UHPLC-QTOF-MS and UHPLC-MS. Our data provide new insights into the ASFV-host interactions, which may help with determination of the infection mechanism of ASFV.

Here, we provide data on the alteration of metabolites and associated pathways in PAMs after ASFV infection. The results of OPLS-DA and hierarchical clustering revealed significant changes in the global metabolite profiles after ASFV infection. As a whole, there were significant changes in amino acids and TCA cycle metabolism, which partly reflect the intracellular contributions to the understanding of how ASFV regulates host metabolism to promote self-replication.

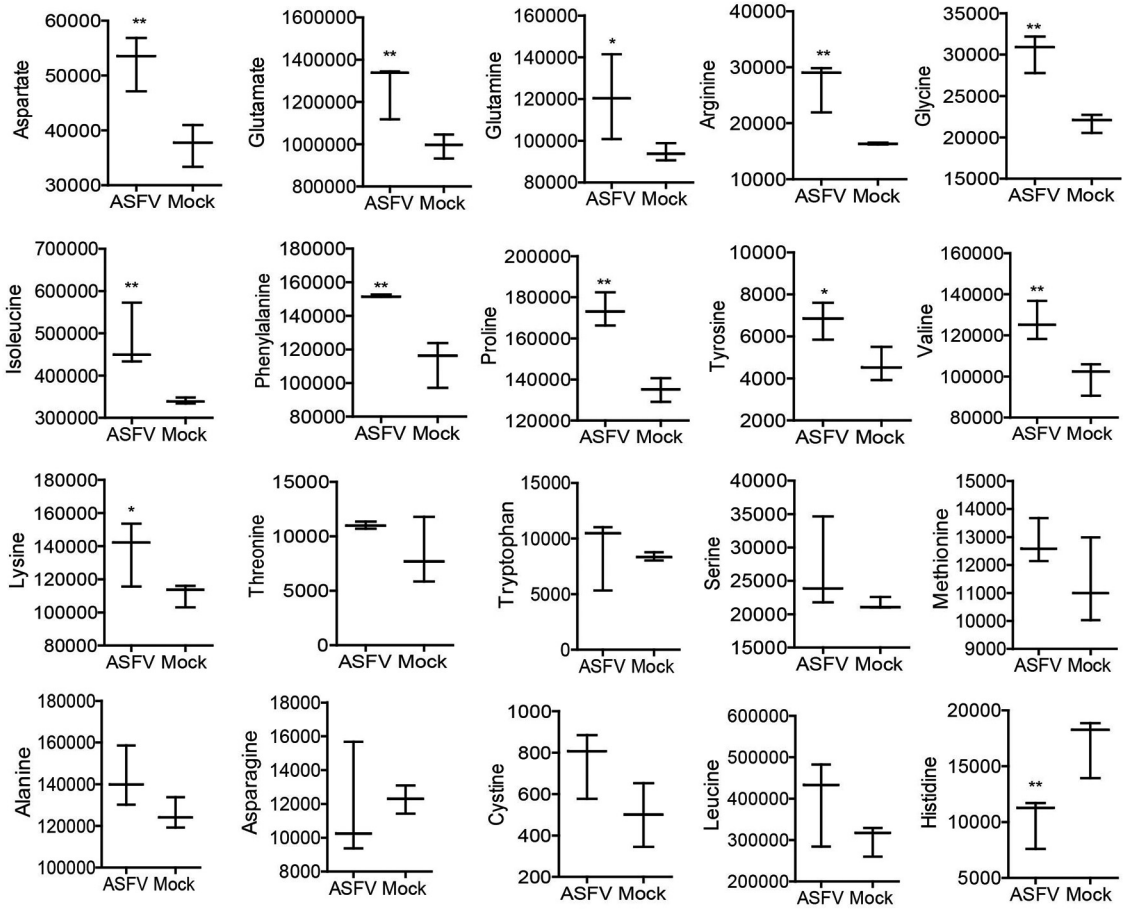

FIG 7 Amino acid metabolism regulated by ASFV infection. PAMs cultured in 6-cm dishes were infected with ASFV (MOI, 1) for 0 or 24 h. The amount of amino acids was quantified by UHPLC-MS. The samples were prepared in parallel three times. Many amino acids were significantly altered in PAMs after ASFV infection. Results are means and standard deviations.

Amino acids are one of the most important substances in cells. They not only are utilized in synthesis of proteins and other important biomolecules but also provide primary substances for other metabolic pathways. Metabolic disorders of amino acids can lead to a variety of diseases. The impact of viral infection on amino acid metabolism has been described for several viruses. For instance, about 300 metabolites are altered significantly in NDV-infected cells, and most of them belong to the amino acid metabolic pathway. Tyrosine, threonine, isoleucine, serine, methionine, and alanine are upregulated, which indicates that these amino acids may play important roles in key metabolic pathways during NDV infection (12). Vaccinia virus (VACV) infection alters glutamine metabolism. Decreasing the exogenous glutamine in VACV-infected cells leads to a significant decrease of infectious virus production, suggesting that glutamine is essential for VACV replication (33). Amino acid metabolism generally increases in Kaposi's sarcoma-associated herpesvirus (KSHV)-infected cells, and KSHV infection activates the Myc pathway to induce glutamine uptake and glutaminolysis to produce TCA cycle intermediates (34, 35). In the present study, we found that large amounts of amino acids were significantly upregulated in the early stages of ASFV infection. However, in the late stages of infection, cellular amino acids were depleted by ASFV. The significant changes in the cell metabolites at 48 hpi may be due to the occurrence of intracellular apoptosis. Detailed analyses confirmed that the aspartate and glutamate promoted ASFV replication, which demonstrated that the increased amount of amino acids contributed to the rapid ASFV protein synthesis and virion assembly.

In addition to amino acid metabolism, glycolysis, TCA cycle, and lipid metabolism also play important roles in viral replication (36). For instance, Marek's disease virus

TABLE 1 Impact of ASFV infection on amino acid levels at 48 hpi

		Concentration of amino acid (nmol)					
Amino acid	***P* value**	**Mock-1**	**Mock-2**	**Mock-3**	**ASFV-1**	**ASFV-2**	**ASFV-3**
Tryptophan	0.000028	1.7469	1.5818	1.76407	0.30797	0.27063	0.36866
Phenylalanine	0.000049	7.5188	7.0271	7.65006	2.68424	2.54517	3.08539
Histidine	0.000070	4.4486	4.6536	4.95475	1.74255	1.62672	1.9335
Valine	0.000199	11.551	11.539	13.2117	4.45473	4.02671	4.71257
Leucine	0.000268	14.908	15.125	17.1451	6.15553	5.90682	6.93775
Isoleucine	0.000294	6.2783	6.335	6.92764	3.31969	2.93448	3.5523
Lysine	0.000379	12.977	13.881	15.649	4.95611	4.57971	5.49141
Serine	0.000444	19.956	20.403	23.6856	8.01948	7.49508	8.8899
Tyrosine	0.000454	6.8623	7.0888	8.13162	2.87423	2.83231	3.25932
Glutamine	0.000536	26.214	23.509	26.2469	12.1498	11.7613	14.4607
Methionine	0.000551	3.7868	4.1028	4.69937	1.47437	1.33436	1.52805
Proline	0.000906	6.6421	6.8434	8.10792	2.93362	2.77946	3.22939
Threonine	0.001070	9.9163	10.566	12.504	4.17185	4.07792	4.60001
Alanine	0.001108	16.047	17.659	20.5587	6.24481	6.72196	7.27285
Asparagine	0.001577	9.7023	9.4915	11.5961	4.70666	4.78759	5.32603
Aspartate	0.005257	8.2874	7.6119	8.93764	5.60539	6.18958	6.05862
Glutamate	0.015470	23.819	21.224	24.592	18.2256	17.5333	19.5538
Arginine	0.029972	1.2657	1.6701	2.60009	0.46461	0.46408	0.65026
Glycine	0.036663	42.725	41.169	45.7276	36.5468	35.3865	39.9523
Cystine	0.369390	0.6793	1.0288	1.42136	0.79142	0.7636	0.91053

(MDV) infection activates an anaplerotic substrate from glucose to glutamine to provide energy and metabolites required for MDV replication (37); DENV-induced autophagy regulates cellular lipid metabolism, leading to an autophagy-dependent processing of lipid droplets and triglycerides to release free fatty acids, which are required for efficient DENV replication (38); and lipid metabolism affects hepatitis C virus (HCV) assembly and entry as well. Specifically, lipoproteins are involved in the entry process, and the cholesterol transporter SR-BI is a key cellular entry factor for HCV (39). The TCA cycle is the hub of carbohydrate, lipid, and amino acid metabolism and plays important roles in many cellular bioprocesses. The TCA cycle significantly facilitates nervous necrosis virus (40) and avian reovirus replication (41). During human cytomegalovirus (HCMV) infection, glutaminase and glutamate dehydrogenase are needed to convert glutamine to α-ketoglutarate, and the α-ketoglutarate enters the TCA cycle for viral replication. ATP and viral production could be rescued in glutamine-starved cells using the TCA intermediate α-ketoglutarate, oxaloacetate, or pyruvate, confirming the importance of the TCA cycle in HCMV replication (42). However, the TCA cycle was not important or necessary for infectious spleen and kidney necrosis virus multiplication (43). These results showed that the TCA cycle plays multiple roles in viral replication.

The ATP-binding cassette transporter A1, which regulates cholesterol metabolism, is upregulated in ASFV-infected pigs (44); the cholesterol in cellular membranes is essential for ASFV infection (45), and the lipid exchange facilitates the formation of vi-

TABLE 2 Impact of ASFV infection on glycolysis[a]

Metabolites	*p*-value	Mock-1	Mock-2	Mock-3	ASFV-1	ASFV-2	ASFV-3
Pyruvate	< 0.05	531367	515426	506659	710257	589554	663336
Fructose 6-phosphate	< 0.05	2526503	3860869	2648236	804892	751848	579864
3-phosphoglycerate	> 0.05	3950167	4652347	4487289	5130192	5290786	4741920
2-phosphoglycerate	> 0.05	3148103	5299043	3751668	4771576	4248797	4022640
Fructose 1,6-bisphosphate	> 0.05	4250941	4353130	5443597	3506461	6009398	8267280
Glucose 6-phosphate	> 0.05	564452	2886000	2225254	434323	747357	551448
Glucose	> 0.05	327843	341686	352178	375550	293732	391608

[a]Values are chromatographic peak area. Red, upregulation; green, downregulation; black, unchanged.

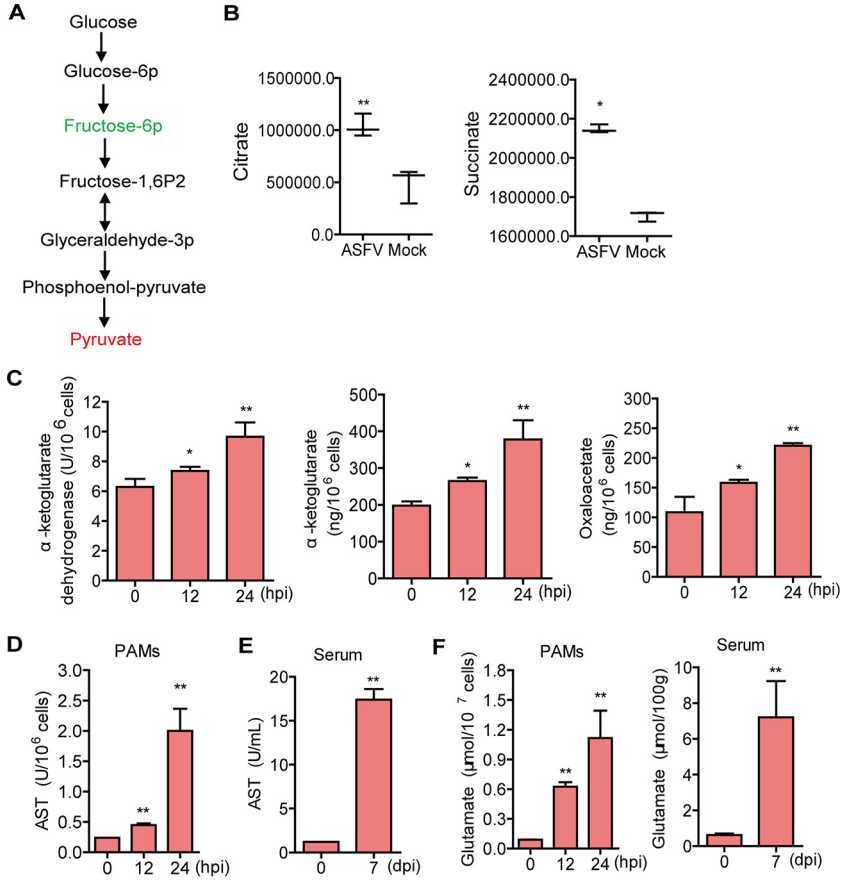

FIG 8 ASFV infection promoted cellular energy metabolism. (A) Schematic representation of altered glycolysis pathways in PAMs infected with ASFV. Red, upregulation; green, downregulation. (B) PAMs were infected with ASFV (MOI, 1) for 24 h. The levels of citrate and succinate were determined by UHPLC-MS. (C) PAMs were infected with ASFV (MOI, 1) for 0, 12, or 24 h. The levels of α-ketoglutarate, α-ketoglutarate dehydrogenase, and oxaloacetate were determined with the appropriate kits. (D) PAMs were infected with ASFV (MOI, 1) for 0, 12, or 24 h. The activity of AST was determined with a kit. (E) The serum was collected from pigs infected with ASFV (7 days after ASFV infection). The activity of AST was determined with a kit. (F) Samples were prepared as described for panels D and E. The level of glutamate was determined with a kit.

rus factories in the context of ASFV infection (46), revealing the importance of lipid metabolism in ASFV infection. Here, our data indicated that the TCA cycle and amino acid metabolism were closely associated with ASFV infection. Pyruvate is the end product of the glycolytic pathway. The pyruvate level was significantly enhanced, while other metabolites in the glycolytic pathway were not increased. The increase in pyruvate

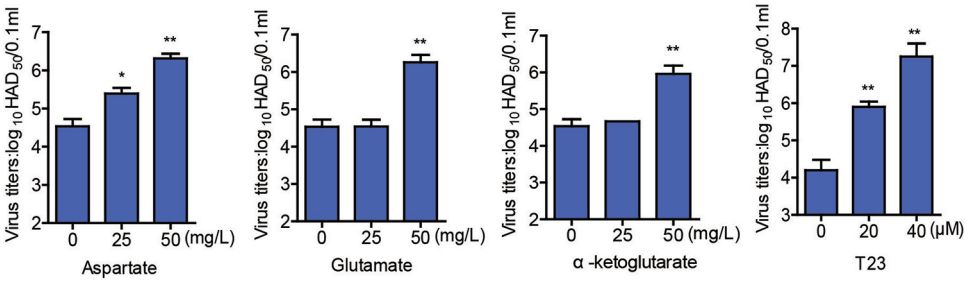

FIG 9 Aspartate, glutamate, and TCA cycle promoted ASFV replication. PAMs cultured in 6-well plates were infected with ASFV (MOI, 1) in the presence of the indicated concentrations of aspartate, glutamate, α-ketoglutarate, or T23. The supernatants were collected, and the viral titers were determined by HAD_{50} assay.

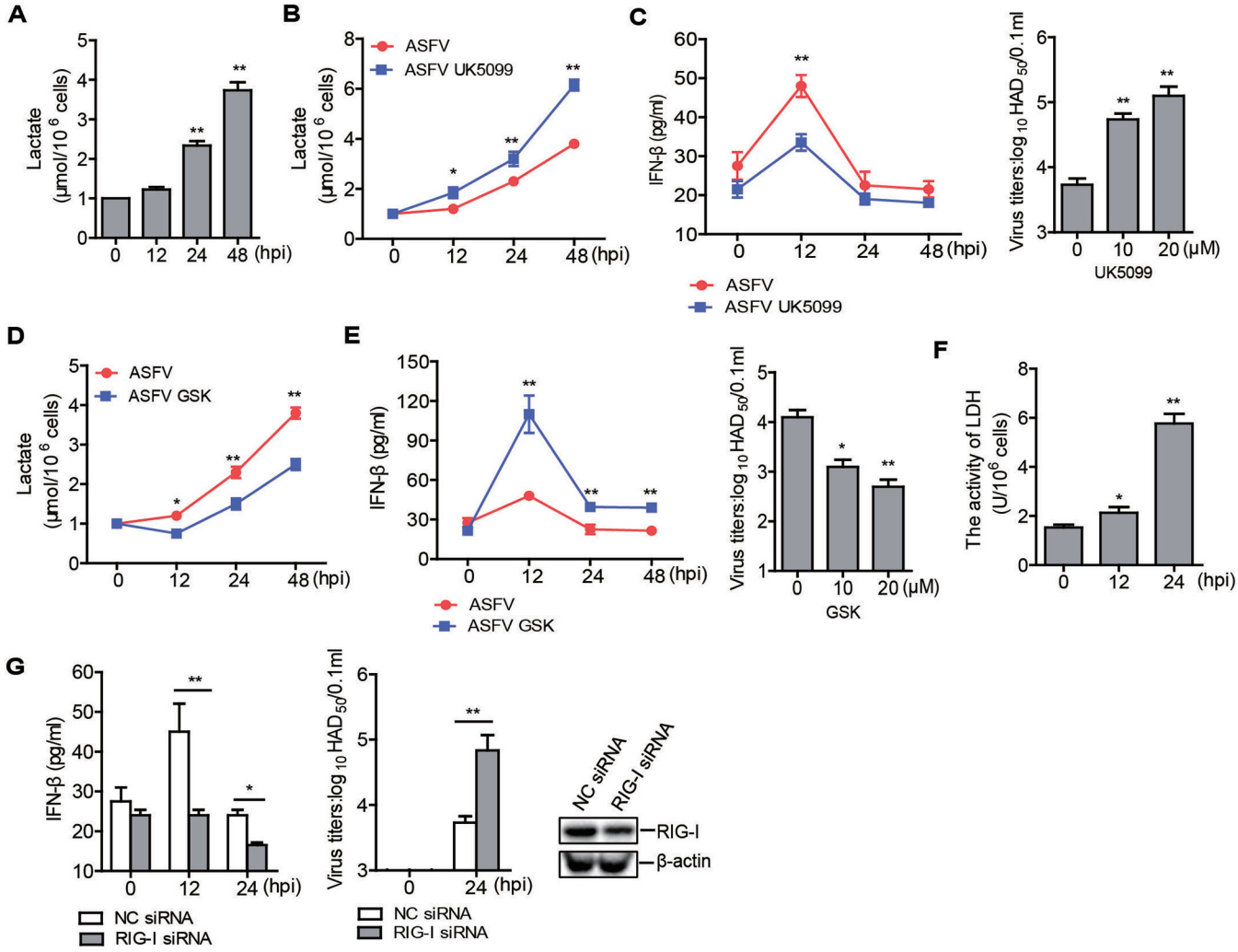

FIG 10 ASFV infection increased lactate production to promote viral replication. (A) PAMs were infected with ASFV (MOI 1) for 0, 12, 24, or 48 h. The levels of lactate were determined with a lactate detection kit. PAMs infected with ASFV (MOI 1) were incubated with and without the inhibitor UK5099 (10 μM) for 0, 12, 24, or 48 h. The levels of lactate were determined with a lactate detection kit (B). The supernatants were collected, and the amounts of secreted IFN-β protein were measured using ELISA (C, left). (C, right) PAMs infected with ASFV (MOI 1) were incubated with 0, 10, or 20 μM inhibitor UK5099 for 24 h. The supernatants were collected and the viral titers were determined by HAD_{50} assay. PAMs infected with ASFV (MOI 1) were incubated with or without the inhibitor GSK (10 μM) for 0, 12, 24, or 48 h. The levels of lactate were determined with a lactate detection kit (D). The amounts of secreted IFN-β protein were measured using an ELISA kit (E, left). (E, right) PAMs infected with ASFV (MOI 1) were incubated with 0, 10, or 20 μM GSK for 24 h. Viral titers were determined by HAD_{50} assay. (F) PAMs were infected with ASFV (MOI 1) for 0, 12, or 24 h. The activity of LDH was determined with an LDH activity assay kit. (G) PAMs were transfected with 250 nM RIG-I siRNA or NC siRNA. At 36 h after transfection, cells were infected with ASFV (MOI 1) and were collected at the indicated time points. The amounts of secreted IFN-β protein were measured using an ELISA kit, viral titers were determined by HAD_{50} assay, and expression of the RIG-I protein was detected by Western blotting.

may be due to the increased TCA cycle and amino acid metabolism. We found that the TCA cycle intermediates, including citrate, succinate, α-ketoglutarate, and oxaloacetate, were significantly increased during ASFV infection, indicating that ASFV infection promoted the TCA cycle. In turn, the TCA cycle was critical for replication of ASFV. The TCA cycle can promote amino acid production under the regulation of several specific enzymes. Therefore, the increase of ASFV replication induced by the TCA cycle may be due to the increase in both ATP and amino acid production.

Lactate directly binds to the MAVS protein transmembrane domain and prevents MAVS protein aggregation, resulting in the inhibition of RLR signaling pathway activation (28). The energy metabolism regulates innate immunity during viral infection. Hepatitis B virus (HBV) infection enhances the production of lactate, which prevents MAVS protein aggregation and mitochondrial localization, resulting in the immune evasion of HBV (47). In the present study, ASFV infection induced a considerable

increase in lactate as well. The increase in lactate level significantly induced low expression of IFN-β, resulting in enhancement of ASFV replication. In addition, RIG-I-regulated ASFV induced the activation of IFN-β. ASFV, as a double-stranded DNA virus, is recognized by cGAS (20). Our results indicated that except for the cGAS-STING pathway, ASFV infection also controls IFN-β production through RIG-I-mediated signaling pathways. Together, our data identified a novel antagonistic mechanism by which ASFV blocks type I IFN production.

There is a discrepancy in the effects of IFN on ASFV replication. Golding et al. reported that porcine IFN-α does not affect the replication of virulent ASFV strains BA71, Georgia 2007/1, and OUR T88/1 in alveolar macrophages (48). Fan et al. found that recombinant porcine IFN-α and IFN-γ have high antiviral activity against ASFV in PAMs (49). Here, our data indicated that porcine IFN-β plays an important role in suppression of ASFV replication. Analysis of the discrepancy indicates that in addition to virus strain, the discrepancy in porcine IFN might be another reason for the different outcome.

In conclusion, ASFV infection could regulate IFN-β production through the RIG-I–MAVS protein signaling pathway. ASFV infection induced the increase of TCA cycle, amino acid production, and pyruvate level. On one hand, the produced pyruvate increased lactate production under the action of LDH, resulting in the immune escape of ASFV. On the other hand, the pyruvate entered and promoted the TCA cycle. The increased TCA cycle then induced the enhancement of ATP and amino acid production, which further promoted ASFV replication (Fig. 11).

African swine fever (ASF) is one of the most serious viral diseases infecting pigs (50). Despite numerous research efforts, there are no available commercial vaccines against ASF (51–56). The development of vaccine has been greatly hindered by the knowledge gaps regarding viral pathogenesis and immune evasion. This work could guide the design of new preventive or therapeutic strategies targeting the altered metabolic pathways and identifies a novel mechanism evolved by ASFV to inhibit host antiviral response.

MATERIALS AND METHODS

Cells and viruses. Porcine alveolar macrophages (PAMs) isolated from healthy pigs were stored in our laboratory (25, 57). PAMs were cultured in RPMI 1640 medium (Gibco) containing 15% inactivated FBS and maintained at 37°C (5% CO_2). The ASFV strain, a genotype II strain named ASFV CN/GS/2018, was isolated and stored in our laboratory (31).

Preparation of aspartate–glutamate–α-ketoglutarate medium. Aspartate (SA8560), glutamate (YZ-100023), and α-ketoglutarate (SK8210) were purchased from Solarbio, Beijing, China. Aspartate, glutamate, and α-ketoglutarate were dissolved in Dulbecco's modified Eagle medium (DMEM) (11995065; Gibco) to a final concentration of 100 mg/L, according to the manufacturer's instructions.

Sample collection. PAMs (10^7 cells) were mock infected or infected with ASFV, collected using cell scrapers, and then centrifuged at 1,200 rpm for 5 min at 4°C. The precipitated cells were resuspended in ice-cold phosphate-buffered saline (PBS). The cells were rapidly quenched using 5 volumes of ice-cold quenching solution (60% aqueous methanol, 0.85% [wt/vol] ammonium bicarbonate; pH 7.4), as described previously (58). The samples were centrifuged to remove the supernatant and the pellet was quickly frozen using liquid nitrogen. Finally, the samples were stored at −80°C until metabolomic analysis. For identification of the ASFV infection, both cells and cell culture supernatants were frozen and thawed three times to release the virus and then were centrifuged at 1,200 rpm for 5 min; the supernatants were collected for virus titration, and the cells were lysed for Western blotting. The serum samples collected from ASFV-infected pigs (25) were used to detect metabolites using appropriate kits, according to the manufacturer's protocol.

Virus titration. The ASFV strains were quantified using the HAD assay, as described previously (25). Briefly, PAMs were cultured in 96-well plates, and the samples were then added to the 96-well plates and titrated in triplicate using 10-fold serial dilutions. HAD_{50} doses were calculated using the Reed and Muench method (59).

Western blotting. The target proteins were analyzed by 10% sodium dodecyl sulfate-polyacrylamide gel electrophoresis (SDS-PAGE) and transferred to nitrocellulose membranes (EMD Millipore, Billerica, MA, USA). The membranes were then blocked with 5% skim milk in Tris-buffered saline–Tween (TBST) at room temperature for 2 h and incubated with appropriate primary antibody (1:1,000) at 4°C overnight and secondary antibody (1:5,000) at room temperature for 2 h. Antibody-antigen complexes were visualized with chemiluminescence detection reagents (Share-bio Biotechnology, Shanghai, China).

Analysis of apoptosis by TUNEL assay. Cellular apoptosis was detected with a TUNEL assay, as described previously (60). Briefly, the PAMs were infected with ASFV (MOI, 1) for 0, 16, 24, or 48 h. The cells were washed once with PBS and were fixed with 4% paraformaldehyde for 30 min. After that, the

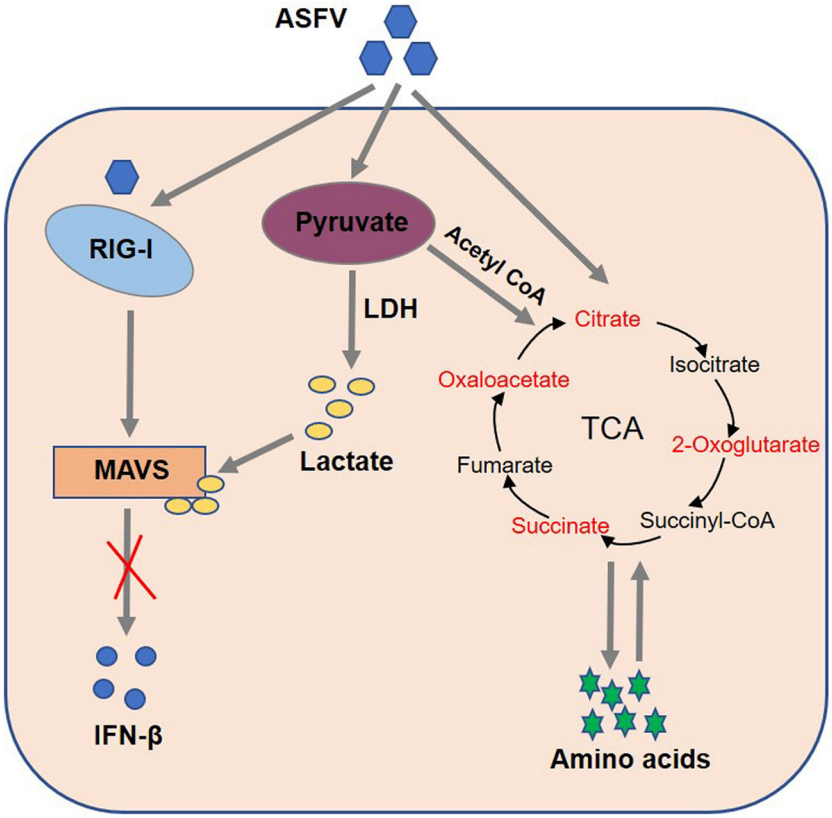

FIG 11 Schematic overview of the working model of how ASFV infection regulates host metabolism. ASFV infection induces the increase in the TCA cycle, amino acid production, and pyruvate level. On one hand, the increased pyruvate causes lactate production under the action of LDH, resulting in the immune evasion by ASFV. On the other hand, the pyruvate enters and promotes the TCA cycle. The increased TCA cycle induces the enhancement of ATP and amino acid production, which further promotes ASFV replication.

cells were incubated with 0.3% Triton X-100 for 5 min at room temperature. Then, the cells were incubated with TUNEL detection liquid (Beyotime, Shanghai, China), according to the manufacturer's instructions. The fluorescence was visualized using a Nikon Eclipse 80i fluorescence microscope.

Knockdown of RIG-I using siRNA. siRNA used in this study was synthesized by Gene Pharma (Shanghai, China). Knockdown of RIG-I in PAMs was performed by transfection of RIG-I siRNA using Polyplus transfection reagent (Jet-PEI, San Marcos, CA, USA) according to the manufacturer's protocol. NC siRNA was used as a negative control. The porcine RIG-I siRNA sequence was as described previously (61). The target sequence for porcine RIG-I was 5′-GGTACAAAGTTGCAGGTAT-3′.

Metabolite extraction. After the samples were slowly thawed at 4°C, 250 μL precooled methanol-acetonitrile-water solution (2:2:1, vol/vol) was added to the Eppendorf tubes and mixed by vortexing for 20 s. Then, the samples underwent ultrasound treatment for 15 min in ice water and were centrifuged at 14,000 rpm for 20 min at 4°C. The supernatant was vacuum dried. During mass spectrometry, 100 μL acetonitrile-water (1:1 [vol/vol]) solution was added to the Eppendorf tubes and vortexed for 2 s. The samples were then centrifuged at 14,000 $\times$ *g* at 4°C for 15 min. The supernatant was collected for further analysis.

Data acquisition through LC-MS analysis. The collected supernatant was separated using Agilent 1290 infinity LC ultrahigh-pressure liquid chromatography (UHPLC), with a column temperature of 25°C, flow rate of 0.5 mL/min, and sample volume of 2 μL. The mobile phase contained A (water, 25 mM ammonium acetate, and 25 mM ammonia) and B (acetonitrile). The gradient elution procedure was as follows: 0 to 0.5 min, 95% B; 0.5 to 7 min, B was decreased linearly from 95 to 65%; 7 to 8 min, B was decreased linearly from 65 to 40%; 8 to 9 min, B was maintained at 40%; 9 to 9.1 min, B was increased linearly from 40 to 95%; 9.1 to 12 min, B was maintained at 95%. The samples were placed in a 4°C autosampler and analyzed in random order. QC samples were inserted into the sample queue to monitor and evaluate the stability of the system and the reliability of the experimental data.

The electrospray ionization (ESI) positive and negative ion modes were used for mass spectrometer (MS) detection. Spectrograms were collected using an AB Triple TOF 6600 mass spectrometer (AB SCIEX, Danaher, Washington, DC, USA). The parameters of the MS were as follows: ion source gas 1: 60; ion source gas 2: 60; curtain gas (CUR): 30; source temperature: 600°C, ion spray voltage floating (ISVF): $\pm$5,500 V; TOF MS scan *m/z* range: 60 to 1,000 Da; product ion scan *m/z* range: 25 to 1,000 Da; TOF MS scan accumulation at time 0.20 s/spectra; product ion scan accumulation at time 0.05 s/spectra. The

parameters of the information dependent acquisition (IDA) were as follows: exclude isotopes with 4 Da; candidate ions to monitor per cycle: 10.

Amino acid metabolism analysis. The ESI positive-ion modes were used for MS detection. The spectrograms were collected using a 5500 QTRAP mass spectrometer (AB SCIEX). The parameters of the MS were as follows: source temperature: 500°C; ion source gas 1: 40; ion source gas 2: 40; CUR: 30; ISVF: 5,500 V.

Energy metabolism analysis. The ESI positive and negative ion modes were used for MS detection. The spectrograms were collected using a 5500 QTRAP mass spectrometer (AB SCIEX). The parameters of the MS in positive ion mode were as follows: source temperature: 500°C; ion source gas 1: 40; ion source gas 2: 50; CUR: 35; ISVF: 5,500 V. The parameters in negative ion modes were as follows: source temperature: 550°C; ion source gas 1: 40; ion source gas 2: 50; CUR: 35; ISVF: −4,500 V.

Metabolite analysis using kits. The activity of AST in PAMs was detected using an aspartate aminotransferase (AST/GOT) activity detection kit (MAK055; Sigma-Aldrich, St. Louis, MO, USA). Alpha-ketoglutarate dehydrogenase and α-ketoglutarate were detected using an A-KG dehydrogenase activity detection kit (MAK189) and an α-ketoglutarate detection kit (MAK054) (Sigma-Aldrich), respectively. Oxaloacetate was detected using an oxaloacetate detection kit (MAK070; Sigma-Aldrich). Glutamate, lactate, and LDH were detected using the corresponding detection kits (BC1580, BC2230, and BC0680, respectively; Solarbio).

ELISA. The expression of porcine IFN-β protein in the cell supernatant was determined using a porcine IFN-β enzyme-linked immunosorbent assay (ELISA) kit (SEKP-0046; Solarbio) according to the manufacturer's instructions. The measured value is compared with that for the standard substance.

MTS assay. To evaluate the cytotoxicity of aspartate, glutamate, α-ketoglutarate, T23, UK5099 (MedChemExpress, Monmouth Junction, NJ), and GSK (MedChemExpress) on cells, an MTS [3-(4,5-dimethylthiazol-2-yl)-5-(3-carboxymethoxyphenyl)-2-(4-sulfophenyl)-2H-tetrazolium] assay was performed according to the manufacturer's protocol.

Statistical analysis. XCMS software (https://xcmsonline.scripps.edu/index.php) was used to analyze the raw data for peak alignment, calibration, and retention time peak area extraction. Accurate mass matching (<25 ppm) was used to identify metabolite structure. Ion peaks with missing values of >50% in the data group were ignored. SIMCA-P 14.1 software package (V14.1; Sartorius Stedim Data Analytics AB, Umea, Sweden) was used for multidimensional statistical analysis, including principal-component analysis (PCA), supervised partial least-squares discriminant analysis (PLS-DA), and orthogonal partial least-squares discriminant analysis (OPLS-DA) (12). The PCA maps, volcano maps, and cluster maps were generated with the R program. KEGG enrichment analysis was utilized to determine the metabolic pathways (62). Single-dimensional statistical analysis was performed using SPSS Statistics for Windows, version 17.0 (SPSS Inc., Chicago, IL, USA). Student's *t* test and variation multiple analyses were used for comparison of the raw data. A *P* value of <0.05 was considered statistically significant; a *P* value of <0.01 was considered statistically highly significant.

ACKNOWLEDGMENTS

We thank the Facility Center Department, Lanzhou Veterinary Research Institute, Shanghai Applied Protein Technology Co., Ltd., and Shanghai Bioprofile Technology Company, Ltd., for technical support during the course of the work.

This work was supported by grants from the National Key R&D Program of China (2021YFD1800100), the National Natural Science Foundation of China (31941002 and 32170161), the Technology Major Project of Gansu Province (20ZD7A006 and NCC0006), and the Chinese Academy of Agricultural Science and Technology Innovation Project (CAAS-ZDRW202006 and CAAS-ASTIP-2021-LVRI) and research funding from the Lanzhou Veterinary Research Institute (CAAS-ASTIP-JBGS-20210101).

We declare that we have no conflict of interest.

REFERENCES

1. Galindo I, Alonso C. 2017. African swine fever virus: a review. Viruses 9:103. https://doi.org/10.3390/v9050103.
2. Dixon LK, Sun H, Roberts H. 2019. African swine fever. Antiviral Res 165:34–41. https://doi.org/10.1016/j.antiviral.2019.02.018.
3. Arzt J, White WR, Thomsen BV, Brown CC. 2010. Agricultural diseases on the move early in the third millennium. Vet Pathol 47:15–27. https://doi.org/10.1177/0300985809354350.
4. Iglesias I, Rodríguez A, Feliziani F, Rolesu S, de la Torre A. 2017. Spatio-temporal analysis of African swine fever in Sardinia (2012-2014): trends in domestic pigs and wild boar. Transbound Emerg Dis 64:656–662. https://doi.org/10.1111/tbed.12408.
5. Zhao D, Liu R, Zhang X, Li F, Wang J, Zhang J, Liu X, Wang L, Zhang J, Wu X, Guan Y, Chen W, Wang X, He X, Bu Z. 2019. Replication and virulence in pigs of the first African swine fever virus isolated in China. Emerg Microbes Infect 8:438–447. https://doi.org/10.1080/22221751.2019.1590128.
6. Bisimwa PN, Ongus JR, Tiambo CK, Machuka EM, Bisimwa EB, Steinaa L, Pelle R. 2020. First detection of African swine fever (ASF) virus genotype X and serogroup 7 in symptomatic pigs in the Democratic Republic of Congo. Virol J 17:135. https://doi.org/10.1186/s12985-020-01398-8.
7. Mur L, Sánchez-Vizcaíno JM, Fernández-Carrión E, Jurado C, Rolesu S, Feliziani F, Laddomada A, Martínez-López B. 2018. Understanding African swine fever infection dynamics in Sardinia using a spatially explicit transmission model in domestic pig farms. Transbound Emerg Dis 65:123–134. https://doi.org/10.1111/tbed.12636.
8. Gaudreault NN, Madden DW, Wilson WC, Trujillo JD, Richt JA. 2020. African swine fever virus: an emerging DNA arbovirus. Front Vet Sci 7:215. https://doi.org/10.3389/fvets.2020.00215.
9. Wang T, Sun Y, Qiu HJ. 2018. African swine fever: an unprecedented disaster and challenge to China. Infect Dis Poverty 7:111. https://doi.org/10.1186/s40249-018-0495-3.
10. Kim HJ, Lee MJ, Lee SK, Kim DY, Seo SJ, Kang HE, Nam HM. 2019. African swine fever virus in pork brought into South Korea by travelers from China, August 2018. Emerg Infect Dis 25:1231–1233. https://doi.org/10.3201/eid2506.181684.

11. Ghazal P, González Armas JC, García-Ramírez JJ, Kurz S, Angulo A. 2000. Viruses: hostages to the cell. Virology 275:233–237. https://doi.org/10.1006/viro.2000.0553.
12. Liu P, Yin Y, Gong Y, Qiu X, Sun Y, Tan L, Song C, Liu W, Liao Y, Meng C, Ding C. 2019. In vitro and in vivo metabolomic profiling after infection with virulent Newcastle disease virus. Viruses 11:962. https://doi.org/10.3390/v11100962.
13. Tian X, Zhang K, Min J, Chen C, Cao Y, Ding C, Liu W, Li J. 2019. Metabolomic analysis of influenza A virus A/WSN/1933 (H1N1) infected A549 cells during first cycle of viral replication. Viruses 11:1007. https://doi.org/10.3390/v11111007.
14. Xi Y, Harwood S, Wise LM, Purdy JG. 2019. Human cytomegalovirus pUL37x1 is important for remodeling of host lipid metabolism. J Virol 93:e00843-19. https://doi.org/10.1128/JVI.00843-19.
15. Joshua CJ. 2019. Metabolomics: a microbial physiology and metabolism perspective. Methods Mol Biol 1859:71–94. https://doi.org/10.1007/978-1-4939-8757-3_3.
16. Goldansaz SA, Guo AC, Sajed T, Steele MA, Plastow GS, Wishart DS. 2017. Livestock metabolomics and the livestock metabolome: a systematic review. PLoS One 12:e0177675. https://doi.org/10.1371/journal.pone.0177675.
17. Parveen M, Miyagi A, Kawai-Yamada M, Rashid MH, Asaeda T. 2019. Metabolic and biochemical responses of Potamogeton anguillanus Koidz. (Potamogetonaceae) to low oxygen conditions. J Plant Physiology 232:171–179. https://doi.org/10.1016/j.jplph.2018.11.023.
18. Zhang H, Ji X, Li P, Liu C, Lou J, Wang Z, Wen W, Xiao Y, Zhang M, Zhu X. 2020. Liquid-liquid phase separation in biology: mechanisms, physiological functions and human diseases. Sci China Life Sci 63:953–985. https://doi.org/10.1007/s11427-020-1702-x.
19. Guo Q, Li F, Duan Y, Wen C, Wang W, Zhang L, Huang R, Yin Y. 2020. Oxidative stress, nutritional antioxidants and beyond. Sci China Life Sci 63:866–874. https://doi.org/10.1007/s11427-019-9591-5.
20. García-Belmonte R, Pérez-Núñez D, Pittau M, Richt JA, Revilla Y. 2019. African swine fever virus Armenia/07 virulent strain controls interferon beta production through the cGAS-STING pathway. J Virol 93:e02298-18. https://doi.org/10.1128/JVI.02298-18.
21. Razzuoli E, Franzoni G, Carta T, Zinellu S, Amadori M, Modesto P, Oggiano A. 2020. Modulation of type I interferon system by African swine fever virus. Pathogens 9:361. https://doi.org/10.3390/pathogens9050361.
22. Zhuo Y, Guo Z, Ba T, Zhang C, He L, Zeng C, Dai H. 2021. African swine fever virus MGF360-12L inhibits type I interferon production by blocking the interaction of importin α and NF-κB signaling pathway. Virol Sin 36:176–186. https://doi.org/10.1007/s12250-020-00304-4.
23. Wang X, Wu J, Wu Y, Chen H, Zhang S, Li J, Xin T, Jia H, Hou S, Jiang Y, Zhu H, Guo X. 2018. Inhibition of cGAS-STING-TBK1 signaling pathway by DP96R of ASFV China 2018/1. Biochem Biophys Res Commun 506:437–443. https://doi.org/10.1016/j.bbrc.2018.10.103.
24. Correia S, Ventura S, Parkhouse RM. 2013. Identification and utility of innate immune system evasion mechanisms of ASFV. Virus Res 173:87–100. https://doi.org/10.1016/j.virusres.2012.10.013.
25. Li D, Yang W, Li L, Li P, Ma Z, Zhang J, Qi X, Ren J, Ru Y, Niu Q, Liu Z, Liu X, Zheng H. 2021. African swine fever virus MGF-505–7R negatively regulates cGAS-STING-mediated signaling pathway. J Immunol 206:1844–1857. https://doi.org/10.4049/jimmunol.2001110.
26. Zou L, Zhao H, Wang D, Wang M, Zhang C, Xiao F. 2014. Expression and purification of a functional recombinant aspartate aminotransferase (AST) from Escherichia coli. J Microbiol Biotechnol 24:998–1003. https://doi.org/10.4014/jmb.1402.02018.
27. Hohnholt MC, Blumrich EM, Waagepetersen HS, Dringen R. 2017. The tricarboxylic acid cycle activity in cultured primary astrocytes is strongly accelerated by the protein tyrosine kinase inhibitor tyrphostin 23. Neurochem Int 102:13–21. https://doi.org/10.1016/j.neuint.2016.11.008.
28. Zhang W, Wang G, Xu ZG, Tu H, Hu F, Dai J, Chang Y, Chen Y, Lu Y, Zeng H, Cai Z, Han F, Xu C, Jin G, Sun L, Pan BS, Lai SW, Hsu CC, Xu J, Chen ZZ, Li HY, Seth P, Hu J, Zhang X, Li H, Lin HK. 2019. Lactate is a natural suppressor of RLR signaling by targeting MAVS. Cell 178:176–189. https://doi.org/10.1016/j.cell.2019.05.003.
29. Herbst EAF, George MAJ, Brebner K, Holloway GP, Kane DA. 2018. Lactate is oxidized outside of the mitochondrial matrix in rodent brain. Appl Physiol Nutr Metab 43:467–474. https://doi.org/10.1139/apnm-2017-0450.
30. Li HM, Guo HL, Xu C, Liu L, Hu SY, Hu ZH, Jiang HH, He YM, Li YJ, Ke J, Long X. 2020. Inhibition of glycolysis by targeting lactate dehydrogenase A facilitates hyaluronan synthase 2 synthesis in synovial fibroblasts of temporomandibular joint osteoarthritis. Bone 141:115584. https://doi.org/10.1016/j.bone.2020.115584.
31. Song W, Peili H, Wei P, Wen H, Daniel CH, Hong W, Hong BH. 2021. DDIT3 Targets Innate Immunity via the DDIT3-OTUD1-MAVS pathway to promote bovine viral diarrhea virus replication. J Virol 95:e02351-20. https://doi.org/10.1128/JVI.02351-20.
32. Fontaine KA, Sanchez EL, Camarda R, Lagunoff M. 2015. Dengue virus induces and requires glycolysis for optimal replication. J Virol 89:2358–2366. https://doi.org/10.1128/JVI.02309-14.
33. Fontaine KA, Camarda R, Lagunoff M. 2014. Vaccinia virus requires glutamine but not glucose for efficient replication. J Virol 88:4366–4374. https://doi.org/10.1128/JVI.03134-13.
34. Singh RK, Lang F, Pei Y, Jha HC, Robertson ES. 2018. Metabolic reprogramming of Kaposi's sarcoma associated herpes virus infected B-cells in hypoxia. PLoS Pathog 14:e1007062. https://doi.org/10.1371/journal.ppat.1007062.
35. Lagunoff M. 2016. Activation of cellular metabolism during latent Kaposi's sarcoma herpesvirus infection. Curr Opin Virol 19:45–49. https://doi.org/10.1016/j.coviro.2016.06.012.
36. Sanchez EL, Lagunoff M. 2015. Viral activation of cellular metabolism. Virology 479–480:609–618. https://doi.org/10.1016/j.virol.2015.02.038.
37. Boodhoo N, Kamble N, Sharif S, Behboudi S. 2020. Glutaminolysis and glycolysis are essential for optimal replication of Marek's disease virus. J Virol 94:e01680-19. https://doi.org/10.1128/JVI.01680-19.
38. Heaton NS, Randall G. 2010. Dengue virus-induced autophagy regulates lipid metabolism. Cell Host Microbe 8:422–432. https://doi.org/10.1016/j.chom.2010.10.006.
39. Popescu CI, Dubuisson J. 2009. Role of lipid metabolism in hepatitis C virus assembly and entry. Biol Cell 102:63–74. https://doi.org/10.1042/BC20090125.
40. Asim M, Jiang S, Yi L, Chen W, Sun L, Zhao L, Khan Khattak MN, Tu J, Lin L. 2017. Glutamine is required for red-spotted grouper nervous necrosis virus replication via replenishing the tricarboxylic acid cycle. Virus Res 227:245–248. https://doi.org/10.1016/j.virusres.2016.11.007.
41. Chi PI, Huang WR, Chiu HC, Li JY, Nielsen BL, Liu HJ. 2018. Avian reovirus σA-modulated suppression of lactate dehydrogenase and upregulation of glutaminolysis and the mTOC1/eIF4E/HIF-1α pathway to enhance glycolysis and the TCA cycle for virus replication. Cell Microbiol 20:e12946. https://doi.org/10.1111/cmi.12946.
42. Chambers JW, Maguire TG, Alwine JC. 2010. Glutamine metabolism is essential for human cytomegalovirus infection. J Virol 84:1867–1873. https://doi.org/10.1128/JVI.02123-09.
43. Guo X, Wu S, Li N, Lin Q, Liu L, Liang H, Niu Y, Huang Z, Fu X. 2019. Accelerated metabolite levels of aerobic glycolysis and the pentose phosphate pathway arr Required for efficient replication of infectious spleen and kidney necrosis virus in Chinese perch brain cells. Biomolecules 9:440. https://doi.org/10.3390/biom9090440.
44. Jaing C, Rowland RRR, Allen JE, Certoma A, Thissen JB, Bingham J, Rowe B, White JR, Wynne JW, Johnson D, Gaudreault NN, Williams DT. 2017. Gene expression analysis of whole blood RNA from pigs infected with low and high pathogenic African swine fever viruses. Sci Rep 7:10115. https://doi.org/10.1038/s41598-017-10186-4.
45. Hernaez B, Alonso C. 2010. Dynamin- and clathrin-dependent endocytosis in African swine fever virus entry. J Virol 84:2100–2109. https://doi.org/10.1128/JVI.01557-09.
46. Galindo I, Cuesta-Geijo M, del Puerto A, Soriano E, Alonso C. 2019. Lipid exchange factors at membrane contact sites in African swine fever virus infection. Viruses 11:199. https://doi.org/10.3390/v11030199.
47. Zhou L, He R, Fang P, Li M, Yu H, Wang Q, Yu Y, Wang F, Zhang Y, Chen A, Peng N, Lin Y, Zhang R, Trilling M, Broering R, Lu M, Zhu Y, Liu S. 2021. Hepatitis B virus rigs the cellular metabolome to avoid innate immune recognition. Nat Commun 12:98. https://doi.org/10.1038/s41467-020-20316-8.
48. Golding JP, Goatley L, Goodbourn S, Dixon LK, Taylor G, Netherton CL. 2016. Sensitivity of African swine fever virus to type I interferon is linked to genes within multigene families 360 and 505. Virology 493:154–161. https://doi.org/10.1016/j.virol.2016.03.019.
49. Fan W, Jiao P, Zhang H, Chen T, Zhou X, Qi Y, Sun L, Shang Y, Zhu H, Hu R, Liu W, Li J. 2020. Inhibition of African swine fever virus replication by porcine type I and type II interferons. Front Microbiol 11:1203. https://doi.org/10.3389/fmicb.2020.01203.
50. Li C, Chai Y, Song H, Weng C, Qi J, Sun Y, Gao GF. 2019. Crystal structure of African swine fever virus dUTPase reveals a potential drug target. mBio 10:e02483-19. https://doi.org/10.1128/mBio.02483-19.
51. Chen W, Zhao D, He X, Liu R, Wang Z, Zhang X, Li F, Shan D, Chen H, Zhang J, Wang L, Wen Z, Wang X, Guan Y, Liu J, Bu Z. 2020. A seven-gene-deleted African swine fever virus is safe and effective as a live attenuated vaccine in pigs. Sci China Life Sci 63:623–634. https://doi.org/10.1007/s11427-020-1657-9.

52. Sun E, Zhang Z, Wang Z, He X, Zhang X, Wang L, Wang W, Huang L, Xi F, Huangfu H, Tsegay G, Huo H, Sun J, Tian Z, Xia W, Yu X, Li F, Liu R, Guan Y, Zhao D, Bu Z. 2021. Emergence and prevalence of naturally occurring lower virulent African swine fever viruses in domestic pigs in China in 2020. Sci China Life Sci 64:752–765. https://doi.org/10.1007/s11427-021-1904-4.
53. Matamoros T, Alejo A, Rodríguez JM, Hernáez B, Guerra M, Fraile-Ramos A, Andrés G. 2020. African swine fever virus protein pE199L mediates virus entry by enabling membrane fusion and core penetration. mBio 11:e00789-20. https://doi.org/10.1128/mBio.00789-20.
54. Borca MV, Ramirez-Medina E, Silva E, Vuono E, Rai A, Pruitt S, Holinka LG, Velazquez-Salinas L, Zhu J, Gladue DP. 2020. Development of a highly effective African swine fever virus vaccine by deletion of the I177L gene results in sterile immunity against the current epidemic Eurasia strain. J Virol 94:e02017-19. https://doi.org/10.1128/JVI.02017-19.
55. Borca MV, Rai A, Ramirez-Medina E, Silva E, Velazquez-Salinas L, Vuono E, Pruitt S, Espinoza N, Gladue DP. 2021. A cell culture-adapted vaccine virus against the current African swine fever virus pandemic strain. J Virol 95:e0012321. https://doi.org/10.1128/JVI.00123-21.
56. Cackett G, Matelska D, Sýkora M, Portugal R, Malecki M, Bähler J, Dixon L, Werner F. 2020. The African swine fever virus transcriptome. J Virol 94:e00119-20. https://doi.org/10.1128/JVI.00119-20.
57. Liu H, Zhu Z, Feng T, Ma Z, Xue Q, Wu P, Li P, Li S, Yang F, Cao W, Xue Z, Chen H, Liu X, Zheng H. 2021. African swine fever virus E120R protein inhibits interferon beta production by interacting with IRF3 to block its activation. J Virol 95:e00824-21. https://doi.org/10.1128/JVI.00824-21.
58. Sellick CA, Hansen R, Stephens GM, Goodacre R, Dickson AJ. 2011. Metabolite extraction from suspension-cultured mammalian cells for global metabolite profiling. Nat Protoc 6:1241–1249. https://doi.org/10.1038/nprot.2011.366.
59. Ramakrishnan MA. 2016. Determination of 50% endpoint titer using a simple formula. World J Virol 5:85–86. https://doi.org/10.5501/wjv.v5.i2.85.
60. Mirzayans R, Murray D. 2020. Do TUNEL and other apoptosis assays detect cell death in preclinical studies? Int J Mol Sci 21:9090. https://doi.org/10.3390/ijms21239090.
61. Zhu Z, Wang G, Yang F, Cao W, Mao R, Du X, Zhang X, Li C, Li D, Zhang K, Shu H, Liu X, Zheng H. 2016. Foot-and-mouth disease virus viroporin 2B antagonizes RIG-I-mediated antiviral effects by inhibition of its protein expression. J Virol 90:11106–11121. https://doi.org/10.1128/JVI.01310-16.
62. Xia J, Sinelnikov IV, Han B, Wishart DS. 2015. MetaboAnalyst 3.0–making metabolomics more meaningful. Nucleic Acids Res 43:W251–257. https://doi.org/10.1093/nar/gkv380.